Ding Min (Orcid ID: 0000-0002-0098-5124)

Soderblom Jason, M. (Orcid ID: 0000-0003-3715-6407)

Bierson Carver, J. (Orcid ID: 0000-0002-6840-7187)

Nimmo Francis (Orcid ID: 0000-0003-3573-5915)

Zuber Maria, T. (Orcid ID: 0000-0003-2652-8017)

Author Manuscript

Constraints on Lunar Crustal Porosity from the Gravitational Signature of Impact Craters

Min Ding[1,†], Jason M. Soderblom[1], Carver J. Bierson[2], Francis Nimmo[2], Colleen Milbury[3], and Maria T. Zuber[1]

[1]Department of Earth, Atmospheric and Planetary Sciences, Massachusetts Institute of Technology, Cambridge, MA 02139, USA

[2]Department of Earth and Planetary Sciences, University of California Santa Cruz, Santa Cruz, CA 95064, USA

[3]Department of Earth, Atmospheric, and Planetary Sciences, Purdue University, West Lafayette, IN 47907, USA

Corresponding author: Min Ding (dingmin@pku.edu.cn)

[†]Current address: School of Earth and Space Sciences, Peking University, Beijing 100871, China

Key Points:

- Crater gravity anomalies are useful for constraining spatial variations in the crustal porosity.

This is the author manuscript accepted for publication and has undergone full peer review but has not been through the copyediting, typesetting, pagination and proofreading process, which may lead to differences between this version and the Version of Record. Please cite this article as doi: 10.1029/2018JE005654

This article is protected by copyright. All rights reserved.

- Western nearside maria and the southern South Pole-Aitken (SP-A) basin are associated with relatively low crustal porosity.
- Southwestern periphery of the nearside maria and surroundings of most large impact basins show relatively high crustal porosity.

Author Manuscript

This article is protected by copyright. All rights reserved.

Abstract

Based on Gravity Recovery and Interior Laboratory (GRAIL) observations and the Lunar Orbiter Laser Altimeter (LOLA) crater database, we constrain the spatial variations in the Moon's crustal porosity (ϕ_c) to a depth of several kilometers using the gravity anomalies of 4,864 mid-sized craters (those with a diameter of 20–100 km). For each crater, we estimated the local ϕ_c by quantifying the gravitational effects of impact-induced porosity change and post-impact breccia infill. The crustal porosity model was uniquely determined assuming a global mean ϕ_c of 12%, although a trade-off exists between the porosity of post-impact breccia infill and the (pre-impact) crustal porosity that results in zero net porosity change underlying the crater floor. At this crustal porosity the effects of impact bulking and compaction compensate each other to yield zero crater residual Bouguer anomaly (RBA), when the effect of post-impact infill is excluded. For lower crustal porosities, bulking dominates to produce a negative RBA; for higher crustal porosities, compaction dominates to produce a positive RBA. Spatial kriging and statistical tests suggest lower-than-average ϕ_c in the western nearside maria and southern South Pole-Aitken (SP-A) basin, in contrast to higher-than-average values in the southwestern periphery of the nearside maria. Most of the large impact basins, presumably formed before the majority of the mid-sized craters we analyzed, show reduced porosities relative to their immediate surroundings.

This article is protected by copyright. All rights reserved.

Author Manuscript

Author Manuscript

Plain Language Summary

Because the Moon lacks plate tectonics and surface erosion, its crustal structure has been preserved since the Late Heavy Bombardment ~ 3.9 billion years ago. The porosity structure of the lunar crust provides critical information on the early cratering history and the formation of major impact basins. Anomalously low crustal porosity implies the existence of relatively young volcanic deposits. In addition, the early porosity evolution of the Moon sheds lights on the origin of life as similar processing acting on the Earth created heat and pore space (as water conduits) to support life on Earth. This study uses 4,864 mid-sized craters as probes into the internal porosity structure of the lunar crust, which is one of the primary objectives of the Gravity Recovery and Interior Laboratory mission. For each mid-sized crater, we inverted the observed crater gravity signature for local crustal porosity. We then applied spatial statistical technique to map the regional-scale variations in the crustal porosity and related the porosity variations with the major geologic units, including the nearside maria, highlands, South Pole-Aitken basin and other impact basins. This study shows that mid-sized craters are useful for detecting regional-scale porosity structure that has long been established in the lunar evolution history.

1 Introduction

Spatial variations in the crustal porosity of the Moon provide critical information for its thermal evolution and cratering history, which can be extrapolated to the terrestrial planets. Variations in the porosity of the lunar highland crust provide insight into the Moon's cumulative cratering history since the pre-Nectarian period, the thermal conductivity of the crust and global

This article is protected by copyright. All rights reserved.

thermal evolution (Ziethe et al., 2009; Laneuville et al., 2013), and the interpretation of heat flux measurements (Langseth et al., 1976; Rasmussen & Warren, 1985; Siegler & Smrekar, 2014) and seismic profiles (Lognonné et al., 2003; Khan et al., 2013). Crustal porosity also influences the chemical and mechanical reaction rates that control geological and ecological evolution (Navarre-Sitchler & Brantley, 2007). Spatial variations in the crustal porosity of the lunar highlands, however, were poorly constrained until the availability of the high quality and resolution lunar gravity model provided by the GRAIL mission (Goossens et al., 2015). Wieczorek et al. (2013) attributed the observed gravity over spherical harmonic degrees 150–310 to surface relief, and solved for crustal density and porosity variations by minimizing the correlation between the topography and Bouguer gravity over 6º-radius cap windows. Besserer et al. (2014) further inverted for the density and porosity vertical gradient over 15º-radius cap windows.

An alternative method to constrain the lunar crustal porosity is to use the gravitational signature of impact craters (Dvorak & Phillips, 1977, 1979; Soderblom et al., 2015; Bierson et al., 2016). Impact craters into typical low to moderate porosity surfaces will increase porosity through brecciation, fracturing and dilatancy (Pilkington & Grieve, 1992; Collins, 2014), whereas impacts into relatively high porosity targets will reduce porosity via localized heating and compaction (Melosh, 1989; Milbury et al., 2015a). The net porosity change determines the observed crater gravity anomaly, or residual Bouguer anomaly (RBA, defined as area-weighted average Bouguer anomaly interior to the crater rim with respect to the average Bouguer anomaly

This article is protected by copyright. All rights reserved.

Author Manuscript

within a background annulus, see 2.1). A regional RBA value of ~ 0 mGal implies a crustal porosity ϕ_r, in which the impact bulking and compaction are in balance (i.e., gravitational effects of the co-existing compacted and bulked crustal structures compensate each other, Milbury et al., 2015a). Regions of the crust with such a porosity will experience minimal impact-related porosity change with time and so can be regarded as in a steady or equilibrium state for a given impactor size-frequency distribution. A large-magnitude non-zero RBA indicates deviation from ϕ_r (ignoring post-impact effects), which implies that the regional crust has not yet reached the steady state. Milbury et al. (2015a) used iSALE impact hydrocode simulations to establish a linear relationship between the crater RBA and the background crustal porosity, yielding a ϕ_r of ~ 7%. Soderblom et al. (2015) compared the observed crater RBA values with local crustal porosities from Wieczorek et al. (2013), supporting this linear relationship but yielding an apparent ϕ_r of ~ 15%. We show that the inconsistency in ϕ_r is largely due to the gravitational effects of highly porous post-impact breccia infill on the observed crater RBA, and therefore reconcile the hydrocode models and observations.

In this study, we used the linear relationship between crater RBA and background crustal porosity, after considering the effects of Bouguer correction and post-impact breccia infill, to estimate local pre-impact ambient crustal porosities (ϕ_c) for 4,864 craters identified in Lunar Orbiter Laser Altimeter (LOLA) data (Head et al., 2010). We then spatially interpolated ϕ_c to map their spatial variations and applied Student's t-test to confirm anomalous regions at a spatial resolution of 5º for the highlands and 10º for the western nearside maria. We also interpolated

Author Manuscript

This article is protected by copyright. All rights reserved.

Author Manuscript

the ratio RBA/D_c (where D_c is the crater diameter) to directly show spatial variations in the crater gravity anomaly, where dividing the crater RBA by D_c removes the crater-size dependence (see Methodology section). It is worth noting that the majority of the observed mid-sized craters (diameters of 20–100 km) must postdate the early formation of regional-scale crustal structure, including the major impact basins (Fassett et al., 2012). In addition, impact-induced porosity changes under the crater floors for these mid-sized craters are distributed almost completely within the crater rims (Collins, 2014; Milbury et al., 2015a). Therefore, the pre-existing regional porosity structure is unlikely to be influenced significantly by these mid-sized craters. The mid-sized craters can thus be used as probes of the regional porosity structure (ϕ_c) that was long been established early in the evolutionary history of the Moon.

2 Methodology

We first calculated the RBA values for 4,864 craters with a crater diameter (D_c) of 20–100 km from the LOLA crater database (Head et al., 2010; Kadish et al., 2011) (Figure 1a). Following Soderblom et al. (2015), the crater RBA is defined as the area-weighted average Bouguer anomaly interior to the crater rim minus the average Bouguer anomaly within a background annulus that extends radially from the outer rim flank (Pike, 1977) (Table 1) to one crater radius beyond the crater rim. The calculated crater RBA was found not to be biased by the existence of ejecta deposits by testing the sensitivity of the crater RBA to the radius of background annulus (Soderblom et al., 2015). We used the GRAIL Bouguer gravity model JGGRAIL_1200C12A_BOUGUER (Goossens et al., 2015), which was derived by assuming a

This article is protected by copyright. All rights reserved.

uniform Bouguer correction density (ρ_0) of 2,550 kg/m^3 (corresponding to a nominal mean crustal porosity of 12%). We filtered the Bouguer gravity model to include spherical harmonic degrees 33–600 and referenced to local topography for each crater. The topographic model is from the LOLA data (Smith et al., 2010). Our crater RBA estimates are consistent with those estimated by applying high-pass filters (Bierson et al., 2016), especially in the spatial pattern (comparing Figure 5a with Figure S2a).

We then forward modeled the Bouguer gravity for each crater, with a focus on the model dependence on the local ambient crustal porosity, ϕ_c. The corresponding local crustal density (ρ_c) is equal to $\rho_g(1-\phi_c)$, where ρ_g is the grain density. Table 1 lists the model parameters and scaling relationships. With a focus on impact-induced porosity change (Region c in Figure 2e), we sequentially modeled three sources of the crater Bouguer anomaly: (a) Bouguer correction using a uniform correction density ρ_0 (equal to the assumed global mean crustal density $\overline{\rho_c}$ and the physical domain is indicated by the green area in Figure 2e), which introduces a non-zero gravity anomaly if $\rho_c \neq \rho_0$ (Figure 2a); (b) post-impact breccia infill, which is typically more porous than the ambient crust (Kiefer et al., 2012, 2015), thus inducing a negative gravity anomaly (Figure 2b); and (c) impact-induced porosity change (the focus of this work). For each crater, we estimated the dimensions of the post-impact infill (blue area in Figure 2e) as the difference between the observed topography and the expected topography for a fresh crater. The fresh-crater topography was determined using the scaling relationships of Pike (1977) and Kalynn et al. (2013) (Table 1, Figure 1c) in a similar manner as Evans et al. (2016). While

This article is protected by copyright. All rights reserved.

Author Manuscript

Author Manuscript

impacts into more porous crust generate slightly smaller craters (Wünnemann et al., 2006; Collins et al., 2011), the effects on the crater gravitational signature will be minor. The physical dimensions of the post-impact infill can be roughly represented by a size-independent parameter, the degradation ratio (*R*) (Forsberg-Taylor et al., 2004), defined as the post-impact infill thickness divided by the expected fresh-crater depth. Figure 1b shows the spatial distribution of *R*. The gravity anomaly of the post-impact infill is controlled by its porosity ($\Delta\phi_f$) relative to that of the local ambient crust, and ρ_g. We calculated the gravity anomalies due to (a) and (b) using Parker's forward modeling method (Parker, 1973) and show the model sensitivity to ρ_g in Figure S3.

For plausible values of ϕ_c, *R*, $\Delta\phi_f$, and ρ_g, the major contributor to the crater Bouguer anomaly is (c) impact-induced porosity change. To estimate the gravitational signature from (c), we re-calculated the crater Bouguer anomalies (Figures 2c) for three impact hydrocode models (Milbury et al., 2015a) with D_c of 46 or 54 km, close to the mean crater diameter of 40 km for our analyzed craters. This re-calculation separates the gravitational signature of (c) impact-induced porosity change due to impact bulking and compaction from that of (a) Bouguer correction, which is necessary for taking into account (b) post-impact infill. We require the Bouguer correction density to vary and be equal to local ρ_c to quantify the gravitational effect solely from (c). We calculated the gravity anomaly by integrating the gravitational attraction from point masses with porosity changes (orange area in Figure 2e), from which we derived the modeled crater RBA. Instead, Milbury et al. (2015a) assumed a uniform Bouguer correction

This article is protected by copyright. All rights reserved.

Author Manuscript

density of 2,650 kg/m^3, and their calculated RBA is to the first order equal to the sum of (a) and (c). Therefore, Milbury et al. (2015a)'s RBA values are notably larger than our re-calculated RBA values solely from (c) (Figure 3a). Further, the dependence of the crater RBA on the integrated crustal column depth reveals that 95% of the crater RBA comes from a depth of 0.15–0.2 D_c (Figure 3b), yielding a depth scale for the local ϕ_c estimate. By further assuming that the RBA is linearly proportional to D_c (Milbury et al., 2015a; Soderblom et al., 2015; Bierson et al., 2016), we derived a linear relationship for the gravity signature from (c): $\frac{RBA}{D_c} = C\rho_g(\phi_c - \phi_r)$, where the model-based parameters ϕ_r and C are estimated to be ~7% and 1.1×10^{-6} mGal·m^2/kg. These two parameters depend on the material strength, porous dilatancy and compaction models, temperature profile, and impact velocity used in the hydrocode model. We could not quantify the associated uncertainty, however, as only three hydrocode simulations were used. Figure 2d shows the total crater Bouguer anomalies for varied ϕ_c values after adding (a), (b), and (c), for a typical crater with R = 0.5, $\Delta\phi_f$ = 10%, ρ_g = 2,900 kg/m^3, and D_c = 54 km. The bold black line in Figure 4a shows the corresponding linear RBA/D_c – ϕ_c relationship. Increasing R, $\Delta\phi_f$, or ρ_g reduces the theoretical RBA/D_c (colored lines in Figure 4a).

In this manner, we establish the RBA/D_c – ϕ_c relationship for each crater based on its D_c and topography (and thus R), assuming a constant $\Delta\phi_f$ of 10%, and a ρ_g of 2,900 kg/m^3 for highland craters and 3,300 kg/m^3 for the mare craters (in the nearside maria). We then inverted the observed RBA/D_c to obtain the local ambient ϕ_c for each crater (black dots in Figure 4b). The scatter in the inverted ϕ_c is primarily due to the variations in R. The global mean RBA/D_c of -

This article is protected by copyright. All rights reserved.

0.07 mGal/km corresponds to a mean ϕ_c of 12%, and the standard deviation of 0.29 mGal/km to 9%. If we assumed a lower $\Delta\phi_f$ of 5%, the corresponding mean ϕ_c becomes 10% with a standard deviation of 8% (Figure 4c). To be consistent with the previous global mean ϕ_c estimate of 12% based on gravity analysis (Wieczorek et al., 2013; Besserer et al., 2014; Han et al., 2014) and Apollo sample and meteorite measurements (Kiefer et al., 2012), we adopted a $\Delta\phi_f$ of 10% for the following spatial analysis. However, sensitivity tests showed that our porosity model is only sensitive to the assumed mean crustal porosity, not to the specific choice of $\Delta\phi_f$ and ϕ_r (Section 3.3).

We applied the moving-window block kriging technique (Cressie, 1993; Hengl, 2007) (Text S1) to map the spatially correlated pattern in the observed RBA/D_c and derived ϕ_c (Figure 5) with standard errors (Figures 6a–b). We chose a cap window radius of 5º for the highlands and 10º for the western nearside maria (encircled by gray curve), based on the density of craters available for our analysis. We excluded mare regions whose spatial extent is too limited for analysis (gray patches). We centered the moving windows at 72×36 grid nodes with a grid distance of 5°. Each window incorporates an average of 10 craters for the highlands and 5 craters for the western nearside maria (Figure S1). Thus, our results for the western-maria region have larger uncertainties. We applied Student's t-test after decoupling transformation (Borgman, 1988) to test the null hypothesis that the local RBA/D_c or ϕ_c are equal to the global means (Figures 6c, 7c). We tested the model sensitivity to the window size by doubling the window radii (Figures S4–5). The kriged maps were validated by deterministic interpolation methods

This article is protected by copyright. All rights reserved.

Author Manuscript

(Ding et al., 2016), including natural neighbor, inverse distance weighted, and Abel-Poisson spline interpolation.

3 Results and Discussion

3.1 Spatial variations in the highlands

Figure 5 shows the kriged maps of RBA/D_c and ϕ_c, and Figure 6 shows the associated standard errors and p-values of the Student's t-tests. The global means of the kriged RBA/D_c and ϕ_c are the same as those of original crater data, while the standard deviations decrease to 0.14 mGal/km and 4%, as the kriging processes have removed the spatially random signals. In the highlands, the southern part of SP-A is associated with the largest negative RBA/D_c of -0.44$\pm$0.10 mGal/km and the lowest ϕ_c of 4$\pm$3% (all errors are the standard errors of the kriged values), suggesting that the local craters probe the impact melt sheet (Vaughan et al., 2013; Hurwitz & Kring, 2014) underlying a relatively thin porous top layer (Besserer et al., 2014), although we cannot exclude the effects of impact-induced porosity decrease and post-impact magmatism (Whitten & Head, 2015; Shearer et al., 2015). The north–south asymmetry of the SP-A basin might be due to enhanced impact melting in the southern half of the basin caused by an oblique impact from north to south with its first contact near the Ingenii basin (Garrick-Bethell & Zuber, 2009; Schultz & Crawford, 2011; Petro, 2012). Alternatively, the positive RBA/D_c anomalies near the Ingenii basin could be caused by post-impact mare deposits (Figure 2b), and thus the inferred high (pre-impact) porosity might be erroneous. In contrast to the SP-A basin, a region immediately to the southwest of the western nearside maria is associated with the highest

This article is protected by copyright. All rights reserved.

Author Manuscript

RBA/D_c of 0.22 ± 0.11 mGal/km and ϕ_c of 21 ± 4 %, probably due to kilometer-scale ejecta deposits emplaced during basin-forming events (Hiesinger, 2006; Petro & Pieters, 2008). The original and kriged RBA/D_c and ϕ_c data are provided in Table S1 and S2.

Other notable anomalies are associated with impact basins 300–900 km in radius (circles in Figure 5). The Moscoviense basin reveals a more negative RBA/D_c and lower ϕ_c interior to the crater rim than the surrounding region (from the crater rim to one crater radius beyond the crater rim), which we confirmed by applying a paired-sample *t*-test at a significance level of 0.05. Paired-sample *t*-tests also suggest porosity reduction for the Apollo, Korolev, Hertzsprung, and Coulomb-Sarton basins. This porosity reduction is consistent with impact-induced compaction and heating (Melosh, 1989; Milbury et al., 2015a) and impact-generated melting (Cintala & Grieve, 1998), while the porosity increase immediately exterior to the basin corresponds to impact ejecta. In contrast, positive RBA/D_c signals in the Humbolditianum, Australe, Orientale, and Ingenii basins are likely due to mare deposits (gray patches, Head, 1976) emplaced after the formation of impact craters, and not a large (pre-impact) ϕ_c.

Figure 7 shows the original and kriged RBA/D_c and ϕ_c data, as well as kriging errors and p-values, along a great-circle cross-section A–F (Figure 5). The results using smaller windows (red curves) are consistent with those using larger windows (blue curves) to the first order. Smaller windows resolve shorter-wavelength variations, e.g., in the Moscoviense basin, while a larger window yields more robust regional estimates with lower kriging errors and p-values. Nevertheless, the p-values at both window sizes (Figures 6c, 7c) suggest that at least the southern

Author Manuscript

This article is protected by copyright. All rights reserved.

SP-A basin is associated with anomalous RBA/D_c at a significance level of 0.05 (i.e., $p < 0.05$). This distinction of the SP-A basin from the rest of the highlands was previously found by gravity admittance analysis (Besserer et al., 2014). We also confirmed a statistical deviation from the global mean in the southwestern periphery of the nearside maria (Figure S5c). The statistical test for ϕ_c showed consistent results.

3.2 Western nearside maria

We estimated an average RBA/D_c of ~ -0.39 mGal/km and ϕ_c of ~ 6% (Figure 5) in the western mare region (including the Mare Imbrium, Oceanus Procellarum, and Mare Nubium), while the craters in the eastern maria are too sparse (Figure 1a) for a reliable estimate. The associated kriging errors (Figures 6a–b, 7a–b) and p-values (Figures 6c, 7c) for the western nearside maria are larger than the highlands due to a sparser crater distribution. We conclude, however, that the western mare region as a whole (with a total of 74 craters) show statistically lower RBA/D_c and ϕ_c values than the global mean values, with a p-value on the order of 10^{-4}.

The largest negative RBA/D_c of -0.70$\pm$0.34 mGal/km and the lowest ϕ_c of 0$\pm$9 % after kriging exists in Mare Imbrium, probably due to the existence of a relatively thick low-porosity top mare layer and/or low-porosity underlying feldspathic crust. A preliminary hydrocode simulation (Milbury et al., 2015b) suggests that a non-porous mare layer of 5 km could reduce the RBA/D_c by ~ 0.3 mGal/km. Therefore, a mare layer of several kilometers should be sufficient to explain the mean RBA/D_c in the Mare Imbrium. However, if the regional mare thickness is only ~ 2 km (De Hon, 1979; Thomson et al., 2009), low-porosity underlying crustal

This article is protected by copyright. All rights reserved.

Author Manuscript

materials would be expected as suggested by Gong et al. (2016). In contrast, the Mare Nubium is associated with slightly positive RBA/D_c and thus relatively high ϕ_c, indicating a thinner mare layer with a higher porosity and/or more porous underlying crust. Post-impact mare deposits may also introduce positive RBA (Evans et al., 2016). We did not find RBA/D_c extremes in Marius Hills, Oceanus Procellarum, where the thickest mare has been suggested (Gong et al., 2016). This is probably due to the limited spatial coverage of mare craters (Figure 1a). The correlation between thick mare basalts (and thus low porosities) and young surface ages (Hiesinger et al., 2011) in the western Mare Imbrium and eastern Oceanus Procellarum implies a scenario that the volcanic eruption starts synchronously (relative to the rate of impacts) and then maintains a constant eruption rate until the observed regional surface age. This correlation also implies that the impact flux during and after mare emplacement was inadequate to notably increase the porosity of the mare layer.

3.3 Model sensitivity and implications

Our porosity (ϕ_c) model depends on the crater diameter range considered (20–100 km for our study), because the depth to which a crater probe is proportional to its size. Our ϕ_c map also relies on the assumed ϕ_r and $\Delta\phi_f$ values. We adopted a ϕ_r of 7% from impact hydrocode simulations (Milbury et al., 2015a) and a $\Delta\phi_f$ of 10% to match the observed global mean crustal porosity $\overline{\phi_c}$ of 12% (Kiefer et al., 2012; Wieczorek et al., 2013). $\overline{\phi_c} > \phi_r$ implies that most of the crust has a high porosity to induce a positive RBA through impact compaction. This is consistent with the existence of a ~10 km thick megaregolith mainly due to basin-scale ejecta

This article is protected by copyright. All rights reserved.

Author Manuscript

deposits (Hörz et al., 1991). However, we find that reducing either $\Delta\phi_f$ or ϕ_r lowers the inferred $\overline{\phi_c}$ (Figure 8). If both $\Delta\phi_f$ and ϕ_r are allowed to vary and $\overline{\phi_c}$ is required to be 12%, the porosity model becomes uniquely determined as it now solely relies on the assumed $\overline{\phi_c}$. This does, however, create a trade-off between $\Delta\phi_f$ and ϕ_r (Figure 8b). It is therefore possible that most of the highland crust has achieved a steady-state in porosity (i.e., $\phi_r = \overline{\phi_c} = 12\%$) if there is a systematic bias in the hydrocode simulations of Milbury et al. (2015a). In this case, the expected porosity of the post-impact breccia infill relative to the ambient crust ($\Delta\phi_f$) is 2%, corresponding to an absolute breccia infill porosity of 14%. This porosity value is entirely possible as it lies within the porosity range of 11–21% from the Apollo impact breccia measurements (Kiefer et al., 2015). We therefore cannot conclude if the highland crust has achieved a steady state in porosity solely from the observed crater gravity anomalies, if a steady state is expected after a prolonged bombardment history.

Our crustal porosity model is more robust in a relative sense given the uncertainty in the input parameters of the iSALE hydrocode models (Milbury et al., 2015a). Our assumption of a depth-independent porosity, instead of a porosity that decreases with depth (Besserer et al., 2013; Wieczorek et al., 2013) may introduce additional errors. Preliminary hydrocode simulations that include a porosity gradient suggest that the crater RBA is most sensitive to the porosity structure of the top few kilometers (Milbury et al., 2015b), implying that the weighted crater probe depth might be less than 0.15–0.2 D_c.

This article is protected by copyright. All rights reserved.

Author Manuscript

In addition to crustal porosity, we have implicitly considered the effects of crater degradation state and post-impact mare deposits on the crater RBA. Other properties are probably less significant: (1) Hydrocode impact models (Milbury et al., 2015a) showed that the crustal thickness is not particularly influential. (2) Regression analysis by Bierson et al. (2016) found no correlation between the crater RBA and the crustal thickness, as well as the grain density (Huang & Wieczorek, 2012; Wieczorek et al., 2013) and crater age. (3) Impact melt sheets have limited influence for D_c less than 100 km (Cintala & Grieve, 1998). (4) Hotter mantle temperatures in the Procellarum KREEP Terrane (Wieczorek & Phillips, 2000; Laneuville et al., 2013; Miljković et al., 2013) may reduce the regional ϕ_r because the hotter temperature reduces the material strength and suppress the creation of pore space (Collins et al., 2004). This implies less porous nearside maria than in this study. However, the spatial pattern should stay the same. (5) Impact characteristics, including impactor composition (material strength and density), size, velocity and angle may contribute significantly to the standard deviations of the RBA/D_c and ϕ_c before kriging. The impact characteristics (e.g., Silber et al., 2017) also influence the fresh crater topography and thus our estimated post-impact infill. However, the theoretical spatial randomness (i.e., lack of correlation) of these impactor parameters means that their effects should be removed by the kriging technique.

A comparison of our porosity model with that of Wieczorek et al. (2013) (Figure S2b) yields a correlation coefficient of 0.59, statistically distinct from zero based on Student's t-test and Fisher transformation. Wieczorek et al. (2013) solved for Bouguer correction densities and

This article is protected by copyright. All rights reserved.

Author Manuscript

corresponding porosities that minimize the correlation between the regional Bouguer anomaly and topography, equivalent to considering only the gravitational source (a) Bouguer correction in our crater gravity method. Thus, our method and the Bouguer correlation method are not entirely independent. The Bouguer correlation method may overestimate the porosity variations for densely cratered regions, as it ignores the gravitational effects of (c) impact bulking and compaction. This overestimation exists in the regions immediately exterior to the Moscoviense and other basins (comparing Figure 5b and S2b). However, the model by Wieczorek et al. (2013) is more accurate for less densely cratered regions such as the Orientale basin (Figures 1, S1a), because our crater gravity-based model depend strongly on the local crater densities (reflected in the standard errors in Figure 6).

The porosity gradient model of Besserer et al. (2014) may overestimate the porosity variations of the pre-impact crust, as they do not consider the gravitational source (c) neither. Although our crater gravity method cannot resolve the spatial variations in the porosity gradient due to the large data scattering, a comparison between Besserer et al. (2014) and our model helps to confirm the depth scale of our porosity model. We calculated the averaged crustal porosity of Besserer's linear porosity model to various depths and found a best-fit depth of ~ 7 km that minimizes the difference between Besserer et al. (2014) and our porosity models (Figure S6). This depth scale is consistent with a mean crater probe depth of 6–8 km, estimated as 0.15–0.2 of the mean crater diameter of 40 km.

This article is protected by copyright. All rights reserved.

Author Manuscript

4 Conclusions

Based on high-resolution GRAIL gravity observations and the extensive LOLA crater database, we developed a method to use the RBA/D_c ratios of the mid-sized craters to map regional-scale spatial variations in the Moon's crustal porosity (ϕ_c), giving insights into the effects of older and larger impact events and nearside volcanism:

1. The analyzed 4,864 mid-sized craters are associated with a mean RBA/D_c of -0.07 mGal/km. The crustal porosity model for the top several kilometers can be uniquely determined assuming a global mean ϕ_c of 12%. Meanwhile, a trade-off exists between the porosity that results in zero net impact-induced porosity change (ϕ_r) and the post-impact infill porosity: Larger ϕ_r implies less porous post-impact breccia infill.

2. In the highlands, the southern SP-A basin shows the largest negative RBA/D_c of -0.44$\pm$0.10 mGal/km and lowest ϕ_c of 4$\pm$3 %, consistent with the existence of an impact melt sheet due to an oblique impact. In contrast, a region immediately to the southwest of the nearside maria is associated with the highest RBA/D_c of 0.22$\pm$0.11 mGal/km and ϕ_c of 21$\pm$4 %, probably due to ejecta deposits emplaced during basin-forming events.

3. Most of the impact basins we investigated, including the Moscoviense, Apollo, Korolev, Hertzsprung, and Coulomb-Sarton basins, show lower porosities interior to the crater rims compared to their surroundings. This is consistent with impact-generated melt sheets and outward emplacement of ejecta deposits. Recovery of the impact basin structures validates our premise that mid-sized craters can be used as probes for regional porosity structure.

This article is protected by copyright. All rights reserved.

Author Manuscript

Author Manuscript

4. The western nearside maria display negative RBA/D_c, consistent with the existence of a top mare layer. The largest negative RBA/D_c of -0.70 ± 0.34 mGal/km exists in the Mare Imbrium, probably due to the combined effects of a thick low-porosity mare layer and low-porosity underlying crust.

Acknowledgements

This study was supported by the GRAIL mission, which is part of NASA's Discovery program and is performed under contract to the Massachusetts Institute of Technology and the Jet Propulsion Laboratory, California Institute of Technology. Gravity and topography models used in this paper are archived in the Geophysics Node of the Planetary Data System. Derived crater statistics and kriged maps are provided in Table S1 and S2 in the Supporting Information. We thank J. C. Andrews-Hanna, J. W. Head, C. M. Pieters, as well as others in the GRAIL team and Brown Planetary group for their constructive comments. We also thank G. Collins, R. Phillips, and B. Johnson for their valuable reviews.

This article is protected by copyright. All rights reserved.

Author Manuscript

References

Besserer, J., Nimmo, F., Wieczorek, M. A., Kiefer, W. S., Andrews-Hanna, J. C., & Zuber, M. T. (2013). Theoretical and observational constraints on lunar mega-regolith thickness. Presented at the 44th Lunar and Planetary Science Conference, The Woodlands, TX, United States.

Besserer, J., Nimmo, F., Wieczorek, M. A., Weber, R. C., Kiefer, W. S., McGovern, P. J., et al. (2014). GRAIL gravity constraints on the vertical and lateral density structure of the lunar crust. *Geophysical Research Letters*, *41*, 5771–5777. https://doi.org/10.1002/2014GL060240

Bierson, C. J., Phillips, R. J., Nimmo, F., Besserer, J., Milbury, C., Keane, J. T., et al. (2016). Interactions between complex craters and the lunar crust: Analysis using GRAIL data. *Journal of Geophysical Research: Planets*, *121*(8). https://doi.org/10.1002/2016JE005090

Borgman, L. E. (1988). New advances in methodology for statistical tests useful in geostatistical studies. *Mathematical Geology*, *20*(4), 383–403.

Cintala, M. J., & Grieve, R. A. F. (1998). Scaling impact melting and crater dimensions: Implications for the lunar cratering record. *Meteoritics & Planetary Science*, *33*(4), 889–912. https://doi.org/10.1111/j.1945-5100.1998.tb01695.x

Collins, G. S. (2014). Numerical simulations of impact crater formation with dilatancy. *Journal of Geophysical Research: Planets*, *119*(12). https://doi.org/10.1002/2014JE004708

This article is protected by copyright. All rights reserved.

Collins, G. S., Melosh, H. J., & Ivanov, B. A. (2004). Modeling damage and deformation in impact simulations. *Meteoritics & Planetary Science, 39*(2), 217–231. https://doi.org/10.1111/j.1945-5100.2004.tb00337.x

Collins, G. S., Melosh, H. J., & Wünnemann, K. (2011). Improvements to the ε -α porous compaction model for simulating impacts into high-porosity solar system objects. *International Journal of Impact Engineering*, *38*(6), 434–439. https://doi.org/10.1016/j.ijimpeng.2010.10.013

Cressie, N. A. C. (1993). Geostatistics. In *Statistics for Spatial Data* (pp. 27–104). Hoboken, NJ: John Wiley & Sons, Inc.

De Hon, R. A. (1979). Thickness of western mare basalts. In *Prec. 10th Lunar Planet. Sci. Conf.* (pp. 2935–2955). New York: Pergamon Press.

Ding, M., Soderblom, J. M., Zuber, M. T., Bierson, C. J., Nimmo, F., & Milbury, C. (2016). Target porosity Controls Crater Residual Bouguer Anomaly in the Lunar Highlands. Presented at the 47th Lunar and Planetary Science Conference, The Woodlands, TX, United States.

Dvorak, J., & Phillips, R. J. (1977). The nature of the gravity anomalies associated with large young lunar craters. *Geophysical Research Letters*, *4*(9), 380–382. https://doi.org/10.1029/GL004i009p00380

This article is protected by copyright. All rights reserved.

Author Manuscript

Author Manuscript

Dvorak, J., & Phillips, R. J. (1979). Analysis of small scale lunar gravity anomalies: Implications for crustal history (pp. 329–331). Presented at the 5th Lunar Planetary Science Conference.

Evans, A. J., Soderblom, J. M., Andrews-Hanna, J. C., Solomon, S. C., & Zuber, M. T. (2016). Identification of buried lunar impact craters from GRAIL data and implications for the nearside maria. *Geophysical Research Letters*, *43*(6), 2445–2455. https://doi.org/10.1002/2015GL067394

Fassett, C. I., Head, J. W., Kadish, S. J., Mazarico, E., Neumann, G. A., Smith, D. E., & Zuber, M. T. (2012). Lunar impact basins: Stratigraphy, sequence and ages from superposed impact crater populations measured from Lunar Orbiter Laser Altimeter (LOLA) data. *Journal of Geophysical Research: Planets*, *117*(E12). https://doi.org/10.1029/2011JE003951

Forsberg-Taylor, N. K., Howard, A. D., & Craddock, R. A. (2004). Crater degradation in the Martian highlands: Morphometric analysis of the Sinus Sabaeus region and simulation modeling suggest fluvial processes. *Journal of Geophysical Research*, *109*(E5), E05002.

Garrick-Bethell, I., & Zuber, M. T. (2009). Elliptical structure of the lunar South Pole-Aitken basin. *Icarus*, *204*(2), 399–408. https://doi.org/10.1016/j.icarus.2009.05.032

Gong, S., Wieczorek, M. A., Nimmo, F., Kiefer, W. S., Head, J. W., Huang, C., et al. (2016). Thicknesses of mare basalts on the Moon from gravity and topography. *Journal of Geophysical Research (Planets)*, *121*, 854–870. https://doi.org/10.1002/2016JE005008

This article is protected by copyright. All rights reserved.

Goossens, S., Frank G. Lemoine, Terence J. Sabaka, Joseph B. Nicholas, Erwan Mazarico, David D. Rowlands, et al. (2015). Global and local gravity field models of the Moon using GRAIL primary and extended mission data. Presented at the 46th Lunar Plan. Sci. Conf., The Woodlands, TX, United States.

Han, S.-C., Schmerr, N., Neumann, G., & Holmes, S. (2014). Global characteristics of porosity and density stratification within the lunar crust from GRAIL gravity and Lunar Orbiter Laser Altimeter topography data: Lunar crustal density and porosity. *Geophysical Research Letters*, *41*(6), 1882–1889. https://doi.org/10.1002/2014GL059378

Head, J. W. (1976). Lunar volcanism in space and time. *Reviews of Geophysics*, *14*(2), 265–300. https://doi.org/10.1029/RG014i002p00265

Head, J. W., Fassett, C. I., Kadish, S. J., Smith, D. E., Zuber, M. T., Neumann, G. A., & Mazarico, E. (2010). Global distribution of large lunar craters: Implications for resurfacing and impactor populations. *Science*, *329*(5998), 1504–1507. https://doi.org/10.1126/science.1195050

Hengl, T. (2007). *A practical guide to geostatistical mapping*. Luxembourg: Office for Official Publications of the European Communities.

Hiesinger, H. (2006). New views of lunar geoscience: An introduction and overview. *Reviews in Mineralogy and Geochemistry*, *60*(1), 1–81. https://doi.org/10.2138/rmg.2006.60.1

Author Manuscript

This article is protected by copyright. All rights reserved.

Hiesinger, H., Head, J. W., Wolf, U., Jaumann, R., & Neukum, G. (2011). Ages and stratigraphy of lunar mare basalts: A synthesis. *Geological Society of America Special Papers*, *477*, 1–51. https://doi.org/10.1130/2011.2477(01)

Hörz, F., Grieve, R., Heiken, G., Spudis, P., & Binder, A. (1991). Lunar surface processes. In G. H. Heiken, D. T. Vaniman, & B. M. French (Eds.), *Lunar Source Book* (pp. 94–96). New York: Cambridge University Press.

Huang, Q., & Wieczorek, M. A. (2012). Density and porosity of the lunar crust from gravity and topography. *Journal of Geophysical Research: Planets*, *117*(E5). https://doi.org/10.1029/2012JE004062

Hurwitz, D. M., & Kring, D. A. (2014). Differentiation of the South Pole–Aitken basin impact melt sheet: Implications for lunar exploration. *Journal of Geophysical Research: Planets*, *119*(6), 2013JE004530. https://doi.org/10.1002/2013JE004530

Kadish, S. J., Fassett, C. I., Head, J. W., D. E. Smith, M. T. Zuber, G. A. Neumann, & E. Mazarico. (2011). A global catalog of large lunar crater (≥20 km) from the Lunar Orbiter Laser Altimeter. Presented at the 42nd Lunar Planetary Science Conference, The Woodlands, TX, United States.

Author Manuscript

This article is protected by copyright. All rights reserved.

Author Manuscript

Kalynn, J., Johnson, C. L., Osinski, G. R., & Barnouin, O. (2013). Topographic characterization of lunar complex craters. *Geophysical Research Letters*, *40*(1), 38–42. https://doi.org/10.1029/2012GL053608

Khan, A., Pommier, A., Neumann, G. A., & Mosegaard, K. (2013). The lunar moho and the internal structure of the Moon: A geophysical perspective. *Tectonophys.*, *609*, 331–352. https://doi.org/10.1016/j.tecto.2013.02.024

Kiefer, W. S., Macke, R. J., Britt, D. T., Irving, A. J., & Consolmagno, G. J. (2012). The density and porosity of lunar rocks. *Geophysical Research Letters*, *39*(7), L07201. https://doi.org/10.1029/2012GL051319

Kiefer, W. S., Macke, R. J., Britt, D. T., Irving, A. J., & Guy J. Consolmagno. (2015). The density and porosity of lunar impact breccias and impact melt rocks and implications for GRAIL gravity modeling of the Orientale impact basin structure. Presented at the 46th Lunar Planetary Science Conference, The Woodlands, TX, United States.

Laneuville, M., Wieczorek, M. A., Breuer, D., & Tosi, N. (2013). Asymmetric thermal evolution of the Moon. *Journal of Geophysical Research: Planets*, *118*(7), 1435–1452. https://doi.org/10.1002/jgre.20103

Langseth, M. G., Keihm, S. J., & Peters, K. (1976). Revised lunar heat-flow values. *Geochimica et Cosmochimica Acta, Supplement*, 3143–3171.

This article is protected by copyright. All rights reserved.

Author Manuscript

Lognonné, P., Gagnepain-Beyneix, J., & Chenet, H. (2003). A new seismic model of the Moon: implications for structure, thermal evolution and formation of the Moon. *Earth and Planetary Science Letters*, *211*(1–2), 27–44. https://doi.org/10.1016/S0012-821X(03)00172-9

Melosh, H. J. (1989). *Impact cratering: a geologic process*. New York: Oxford Univ. Press.

Milbury, C., Johnson, B. C., Melosh, H. J., Collins, G. S., Blair, D. M., Soderblom, J. M., Nimmo, F., & Bierson, C. J. (2015a). Preimpact porosity controls the gravity signature of lunar craters. *Geophysical Research Letters*, *42*. https://doi.org/10.1002/2015GL066198

Milbury, C., Johnson, B. C., Melosh, H. J., Collins, G. S., Blair, D. M., Soderblom, J. M., Nimmo, F., Phillips, R. J., et al. (2015b). The effect of pre-impact porosity and vertical density gradients on the gravity signature of lunar craters as seen by GRAIL. In *Bridging the Gap III: Impact Cratering in Nature, Experiments and Modeling*. Abstract 1085.

Miljković, K., Wieczorek, M. A., Collins, G. S., Laneuville, M., Neumann, G. A., Melosh, H. J., et al. (2013). Asymmetric distribution of lunar impact basins caused by variations in target properties. *Science*, *342*(6159), 724–726. https://doi.org/10.1126/science.1243224

Navarre-Sitchler, A., & Brantley, S. (2007). Basalt weathering across scales. *Earth and Planetary Science Letters*, *261*(1–2), 321–334. https://doi.org/10.1016/j.epsl.2007.07.010

Parker, R. L. (1973). The rapid calculation of potential anomalies. *Geophysical Journal International*, *31*(4), 447–455. https://doi.org/10.1111/j.1365-246X.1973.tb06513.x

This article is protected by copyright. All rights reserved.

Author Manuscript

Petro, N. E. (2012). Formation of South Pole-Aitken basin as the result of an oblique impact: Implications for melt volume and source of exposed materials. Presented at the 43th Lunar and Planetary Science Conference, The Woodlands, TX, United States.

Petro, N. E., & Pieters, C. M. (2008). The lunar-wide effects of basin ejecta distribution on the early megaregolith. *Meteoritics & Planetary Science*, *43*(9), 1517–1529. https://doi.org/10.1111/j.1945-5100.2008.tb01025.x

Pike, R. J. (1977). Size-dependence in the shape of fresh impact craters on the moon. In D. J. Roddy, R. O. Pepin, & R. B. Merrill (Eds.), *Impact and Explosion Cratering: Planetary and Terrestrial Implications* (pp. 489–509). New York: Pergamon Press.

Pilkington, M., & Grieve, R. A. F. (1992). The geophysical signature of terrestrial impact craters. *Reviews of Geophysics*, *30*(2), 161–181. https://doi.org/10.1029/92RG00192

Rasmussen, K. L., & Warren, P. H. (1985). Megaregolith thickness, heat flow, and the bulk composition of the Moon. *Nature*, *313*(5998), 121–124. https://doi.org/10.1038/313121a0

Schultz, P. H., & Crawford, D. A. (2011). Origin of nearside structural and geochemical anomalies on the Moon. In W. A. Ambrose & D. A. Williams (Eds.), *Recent Advances and Current Research Issues in Lunar Stratigraphy: Geological Society of America Special Paper 477* (Vol. 477, pp. 141–159). Geological Society of America. https://doi.org/10.1130/2011.2477(07)

This article is protected by copyright. All rights reserved.

Author Manuscript

Shearer, C. K., Elardo, S. M., Petro, N. E., Borg, L. E., & McCubbin, F. M. (2015). Origin of the lunar highlands Mg-suite: An integrated petrology, geochemistry, chronology, and remote sensing perspective. *American Mineralogist*, *100*(1), 294–325. https://doi.org/10.2138/am-2015-4817

Siegler, M. A., & Smrekar, S. E. (2014). Lunar heat flow: Regional prospective of the Apollo landing sites. *Journal of Geophysical Research: Planets*, *119*(1). https://doi.org/10.1002/2013JE004453

Silber, E. A., Osinski, G. R., Johnson, B. C., & Grieve, R. A. F. (2017). Effect of impact velocity and acoustic fluidization on the simple-to-complex transition of lunar craters. *Journal of Geophysical Research: Planets*, *122*(5), 800–821. https://doi.org/10.1002/2016JE005236

Smith, D. E., Zuber, M. T., Neumann, G. A., Lemoine, F. G., Mazarico, E., Torrence, M. H., et al. (2010). Initial observations from the Lunar Orbiter Laser Altimeter (LOLA). *Geophysical Research Letters*, *37*(18). https://doi.org/10.1029/2010GL043751

Soderblom, J. M., Evans, A. J., Johnson, B. C., Melosh, H. J., Miljković, K., Phillips, R. J., et al. (2015). The fractured Moon: Production and saturation of porosity in the lunar highlands from impact cratering. *Geophysical Research Letters*, *42*(17). https://doi.org/10.1002/2015GL065022

This article is protected by copyright. All rights reserved.

Author Manuscript

Thomson, B. J., Grosfils, E. B., Bussey, D. B. J., & Spudis, P. D. (2009). A new technique for estimating the thickness of mare basalts in Imbrium Basin. *Geophysical Research Letters*, *36*(12). https://doi.org/10.1029/2009GL037600

Vaughan, W. M., Head, J. W., Wilson, L., & Hess, P. C. (2013). Geology and petrology of enormous volumes of impact melt on the Moon: A case study of the Orientale basin impact melt sea. *Icarus*, *223*(2), 749–765. https://doi.org/10.1016/j.icarus.2013.01.017

Whitten, J., & Head, J. W. (2015). Lunar cryptomaria: Mineralogy and composition of ancient volcanic deposits. *Planetary and Space Science*, *106*, 67–81. https://doi.org/10.1016/j.pss.2014.11.027

Wieczorek, M. A., Neumann, G. A., Nimmo, F., Kiefer, W. S., Taylor, G. J., Melosh, H. J., et al. (2013). The crust of the Moon as seen by GRAIL. *Science*, *339*(6120), 671–675. https://doi.org/10.1126/science.1231530

Wieczorek, Mark A., & Phillips, R. J. (2000). The “Procellarum KREEP Terrane”: Implications for mare volcanism and lunar evolution. *Journal of Geophysical Research: Planets*, *105*(E8), 20417–20430. https://doi.org/10.1029/1999JE001092

Wünnemann, K., Collins, G. S., & Melosh, H. J. (2006). A strain-based porosity model for use in hydrocode simulations of impacts and implications for transient crater growth in porous targets. *Icarus*, *180*(2), 514–527. https://doi.org/10.1016/j.icarus.2005.10.013

This article is protected by copyright. All rights reserved.

Ziethe, R., Seiferlin, K., & Hiesinger, H. (2009). Duration and extent of lunar volcanism: Comparison of 3D convection models to mare basalt ages. *Planetary and Space Science*, *57*(7), 784–796. https://doi.org/10.1016/j.pss.2009.02.002

Table 1. Parameter Ranges and Scaling Relationships for Crater Bouguer Gravity Models

Parameter	Description	Range/Equation
D_c	Crater diameter (km)	20–100
D_f	Crater floor diameter (km)	$0.19D_c^{1.25}$*
H	Fresh crater floor depth in the highlands (km)	$1.558D_c^{0.254}$†
	Fresh crater floor depth in the maria (km)	$0.87D_c^{0.352}$†
h	Observed crater floor depth (km)	0–5
R	Crater degradation ratio	$(H-h)/H$
W_R	Width of rim flank (km)	$0.467D_c^{0.836}$*
D_R	Diameter of outer rim flank (km)	$D_c + 2W_R$
$\boldsymbol{h_R}$	Rim height (km)	$0.236D_c^{0.399}$*
$\boldsymbol{\rho_g}$	Highland grain density (kg/m^3)	2,900‡
	Mare grain density (kg/m^3)	3,300‡
$\overline{\boldsymbol{\rho_c}}$	Global mean crustal density (kg/m^3)	2,550§
$\overline{\boldsymbol{\phi_c}}$	Global mean crustal porosity (%)	12§
$\boldsymbol{\rho_0}$	Bouguer correction density (kg/m^3)	2,550
$\Delta\boldsymbol{\phi_f}$	Porosity of post-impact breccia infill wrt. ambient crust (%)	0–10**
$\boldsymbol{\phi_r}$	Crustal porosity that results in zero net impact-induced porosity change and crater RBA (%)	7††

*Pike (1977)
†Kalynn et al. (2013)
‡Huang & Wieczorek (2012)
§Kiefer et al. (2012); Wieczorek et al. (2013); Besserer et al. (2014); Han et al. (2014)
**Kiefer et al. (2015)
††Milbury et al. (2015a)

This article is protected by copyright. All rights reserved.

Author Manuscript

Author Manuscript

Figure Captions

Figure 1. Crater locations and degradation states based on lunar topography. (a) Topography map and locations of 4,864 mid-sized craters from the LOLA crater database used in this study. (b) Map of the kriged crater degradation ratio (*R*). The grid spacing is 10º for the western nearside maria (encircled by the gray curve) and 5º for the rest of the area (same as in Figures 5 and 6). The global mean *R* value of 0.47 corresponds to a partially degraded state, while lower *R* implies younger local craters with a limited amount of post-impact infill. (c) Observed crater floor depth for highland craters (blue dots) and mare craters (red triangles). The blue and red curves are the expected crater floor depth for fresh craters (i.e., R = 0) in the highlands and maria, respectively (Kalynn et al., 2013).

Figure 2. Modeled crater Bouguer gravity due to (a) Bouguer correction assuming a uniform Bouguer correction density, (b) post-impact breccia infill with variable $\Delta\phi_f$, or mare infill with a density of 3,150 kg/m^3, and (c) impact-induced porosity change. (d) Total crater Bouguer anomaly by adding (a), (b), and (c). All the modeled curves are vertically shifted to ensure that the average gravity within the background annulus (i.e., from outer rim flank to one crater radius) is zero; vertical shifts do not influence the crater RBA values. (e) Physical domains corresponding to (a), (b) and (c), indicated by different colors. Bold black curve is the observed topography. Fixed parameters include R = 0.5, D_c = 54 km, $\Delta\phi_f$ = 10%, and ρ_g = 2,900 kg/m^3. The scaling relationships for H, h_R, D_f, and D_R are listed in Table 1, yielding 4.3 km, 1.2 km, 27.8 km, and 81.8 km, respectively. h is the observed crater floor depth, assuming to be 0.5H.

This article is protected by copyright. All rights reserved.

Author Manuscript

Figure 3. Crater gravity and probe depth based on iSALE hydrocode simulations (Milbury et al., 2015a). (a) Crater RBA/D_c ratios solely due to impact-induced porosity changes (corresponding to Figure 2c). Black dots and black line are re-calculated ratios using (varied) Bouguer correction densities equal to crustal densities. Blue dots and blue line are original values from Milbury et al. (2015a) where a constant Bouguer correction density was assumed. Gray dots and dashed line are the results for larger crater diameter of 90 or 96 km. The slope for the larger-diameter models is steeper, but this secondary effect is negligible in this study. (b) Cumulative crater RBA, normalized by the total RBA, over increasing depth column (z) for four impact hydrocode models in Milbury et al. (2015a). Dots indicate the effective depths when 95% of the total RBA is reached.

Figure 4. (a) Modeled RBA/D_c–ϕ_c relationship for variable R, $\Delta\phi_f$, and ρ_g. (b) Observed RBA/D_c ratios and converted ϕ_c assuming $\Delta\phi_f$ = 10%. (c) Histogram of converted ϕ_c assuming $\Delta\phi_f$ = 10% (gray) or 5% (orange).

Figure 5. Maps of the kriged (a) RBA/D_c and (b) ϕ_c in a Lambert azimuthal equal-area projection centered over the nearside (left) and farside (right). The grid spacing is 10º for the western nearside maria (encircled by the gray curve) and 5º for the rest of the area. Gray patches indicate mare basalt deposits (Head, 1976) other than the western nearside maria. Circles indicate major highland basins. Initials SP-A, CS, FS and MR represent South Pole-Aitken, Coulomb-Sarton, Freundlich-Scharonov and Mendel-Rydberg basins, respectively.

This article is protected by copyright. All rights reserved.

Figure 6. Standard errors of the kriged (a) RBA/D_c and (b) ϕ_c values in Figure 5. (c) P-values under the null hypothesis that the regional RBA/D_c are equal to the global mean value of -0.07 mGal/km.

Figure 7. (a) Observed RBA/D_c and (b) converted ϕ_c values before and after kriging along the cross-section A–F (Figure 5). Red solid and dashed lines are the kriged values (corresponding to Figure 5) and errors (Figure 6), respectively, using a window radius of 5º for the highlands and 10º for the western nearside maria. Gray dots are the original data within the local windows. Blue lines correspond to results with doubled window radii (Figures S4–5). (c) P-values under the null hypothesis that the regional RBA/D_c is equal to the global mean. (d) Crustal structure and inferred crustal porosities. Vertical lines indicate the maximum crater probe depth of 0.2D_c for the craters in (a) and (b). The Moho relief is from Wieczorek et al. (2013).

Figure 8. Trade-off between $\Delta\phi_f$ and ϕ_r. (a) Expected linear relationship between the total RBA/D_c and crustal porosity for a typical crater with varied $\Delta\phi_f$ and ϕ_r, assuming R = 0.5, D_c = 54 km, and ρ_g = 2,900 kg/m^3. (b) Mean crustal porosity for varied $\Delta\phi_f$ and ϕ_r. The bold black line indicates the solutions with an assumed global mean crustal porosity of 12%. Our porosity model assumed a ϕ_r of 7% (black dot).

Author Manuscript

This article is protected by copyright. All rights reserved.

Author Manuscript

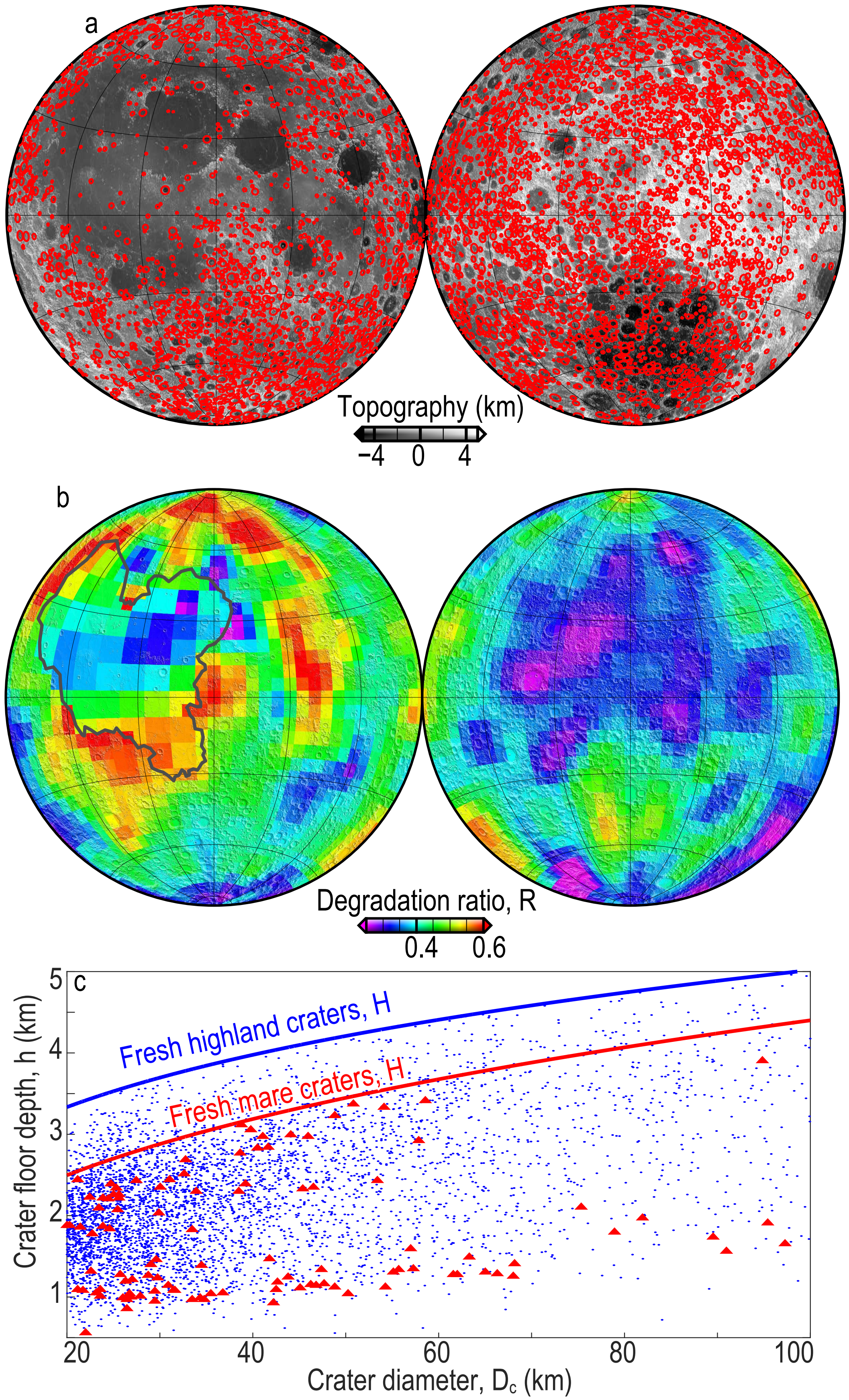

This article is protected by copyright. All rights reserved.

Author Manuscript

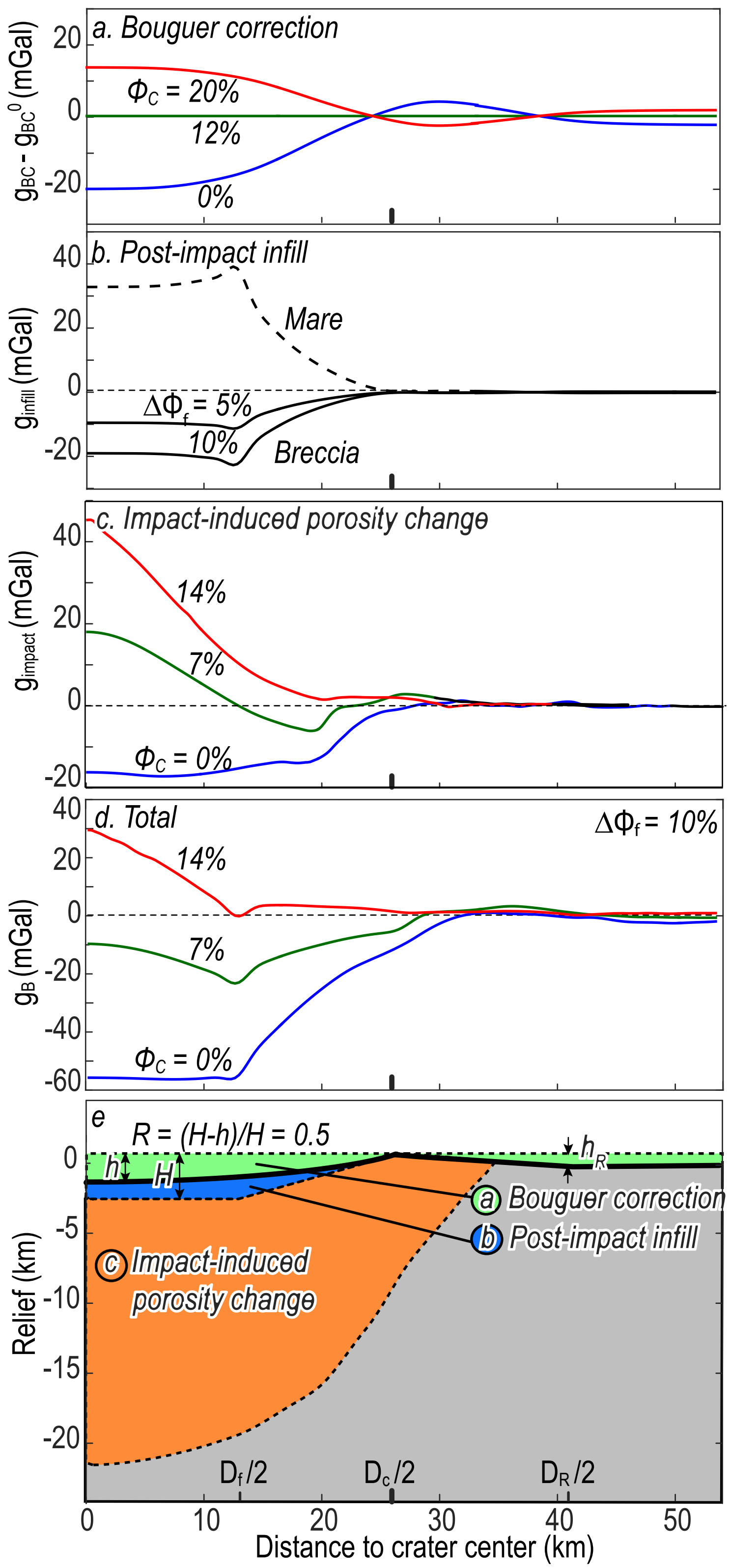

This article is protected by copyright. All rights reserved.

Author Manuscript

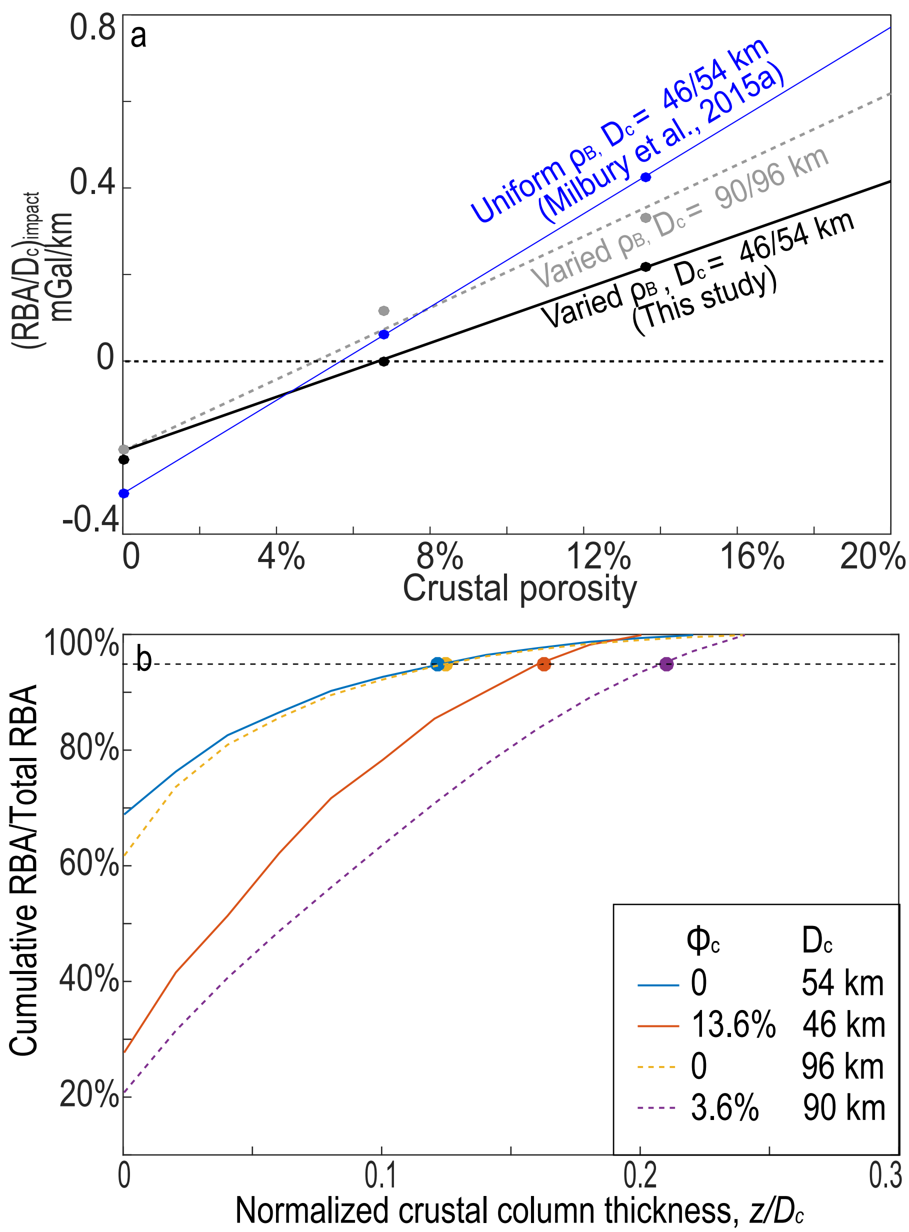

This article is protected by copyright. All rights reserved.

Author Manuscript

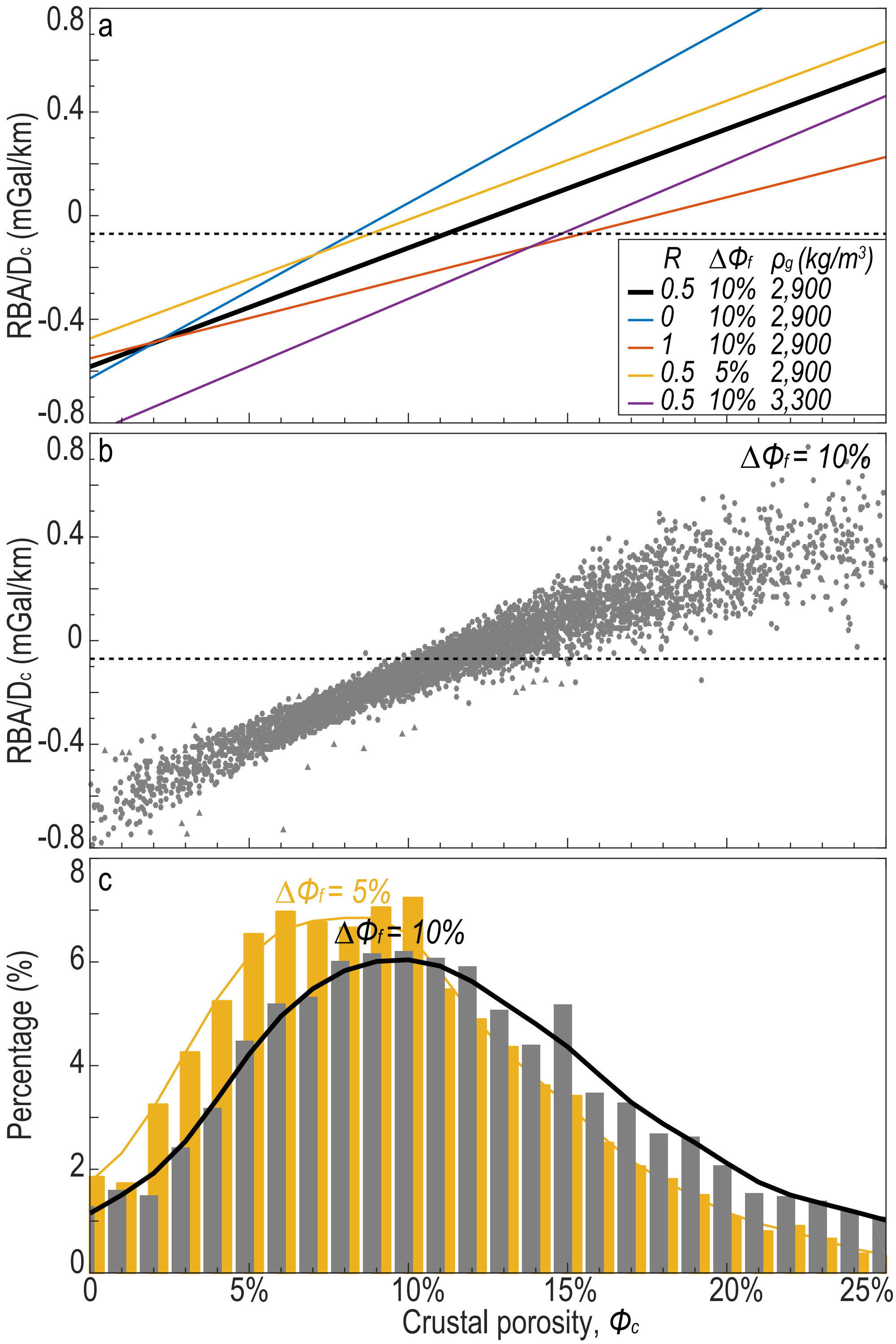

This article is protected by copyright. All rights reserved.

Author Manuscript

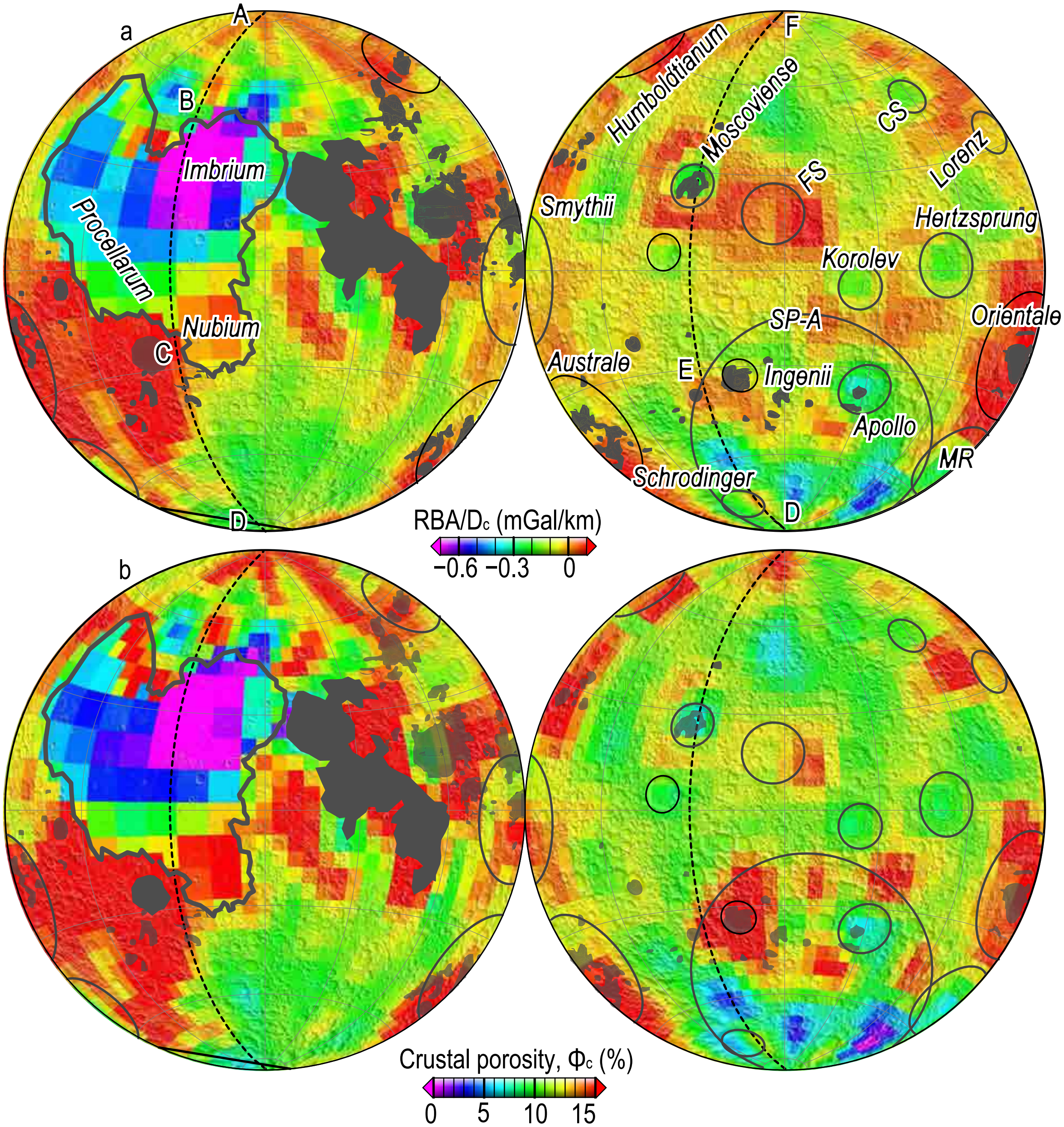

This article is protected by copyright. All rights reserved.

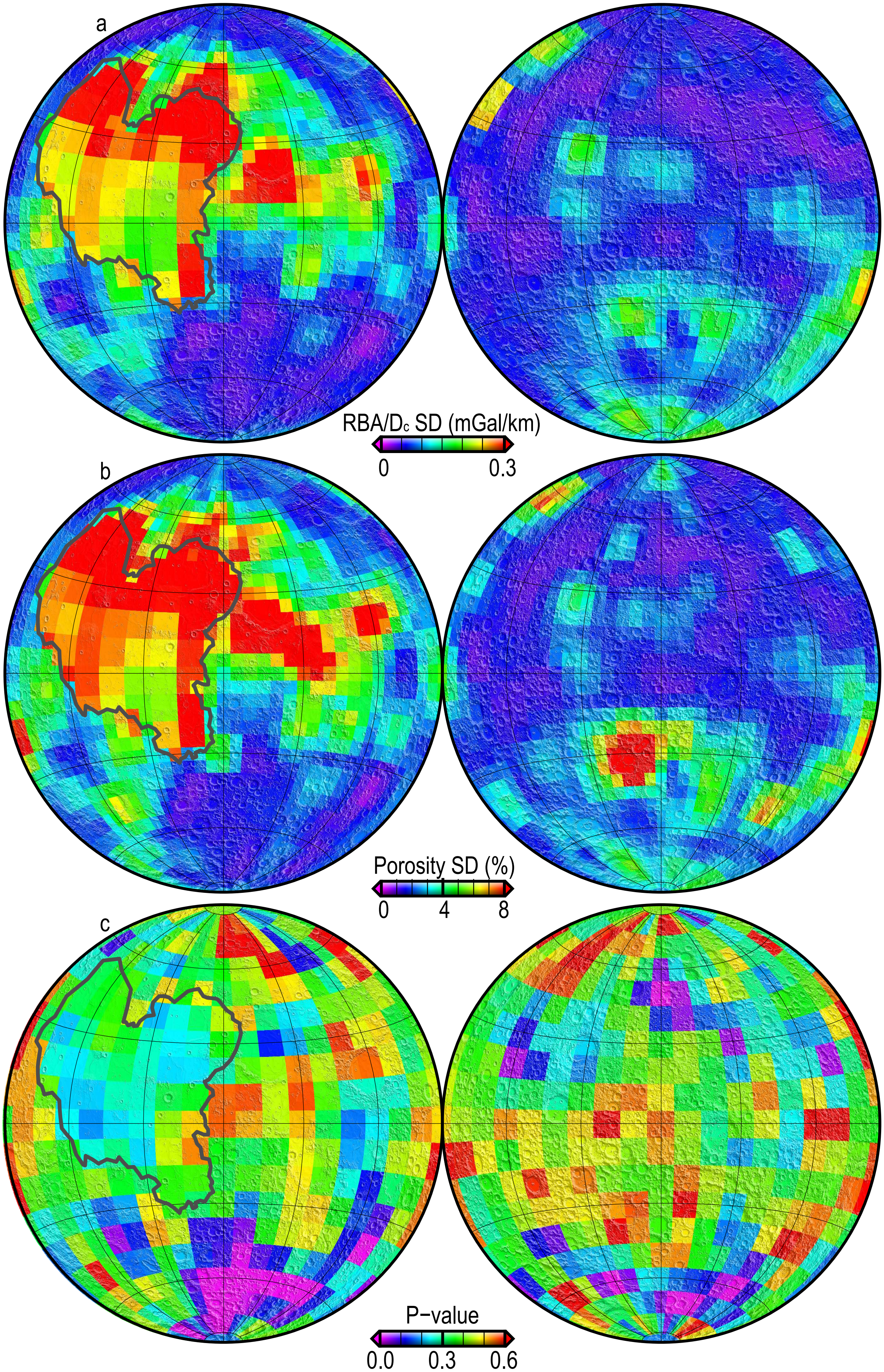

Author Manuscript

This article is protected by copyright. All rights reserved.

Author Manuscript

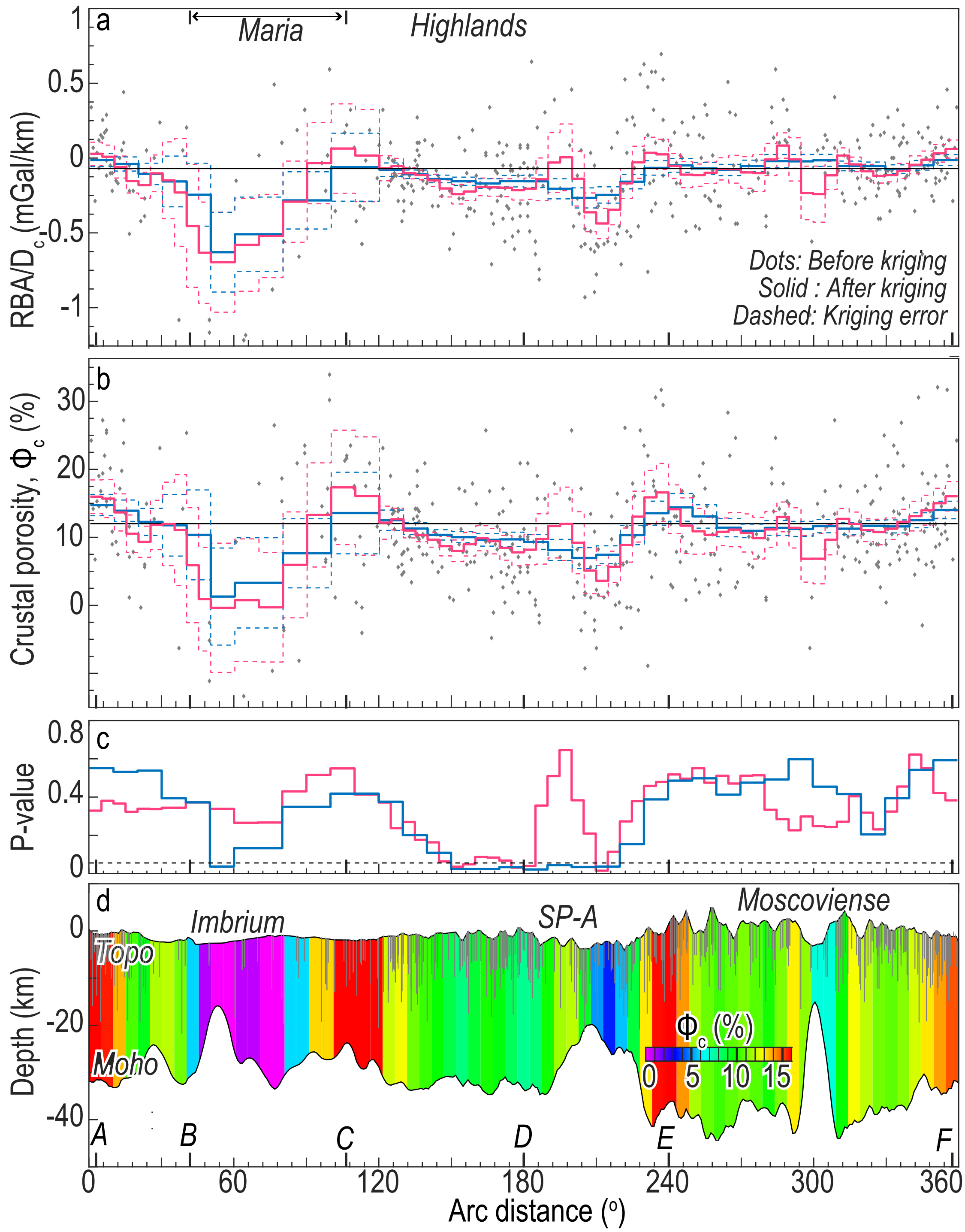

This article is protected by copyright. All rights reserved.

Author Manuscript

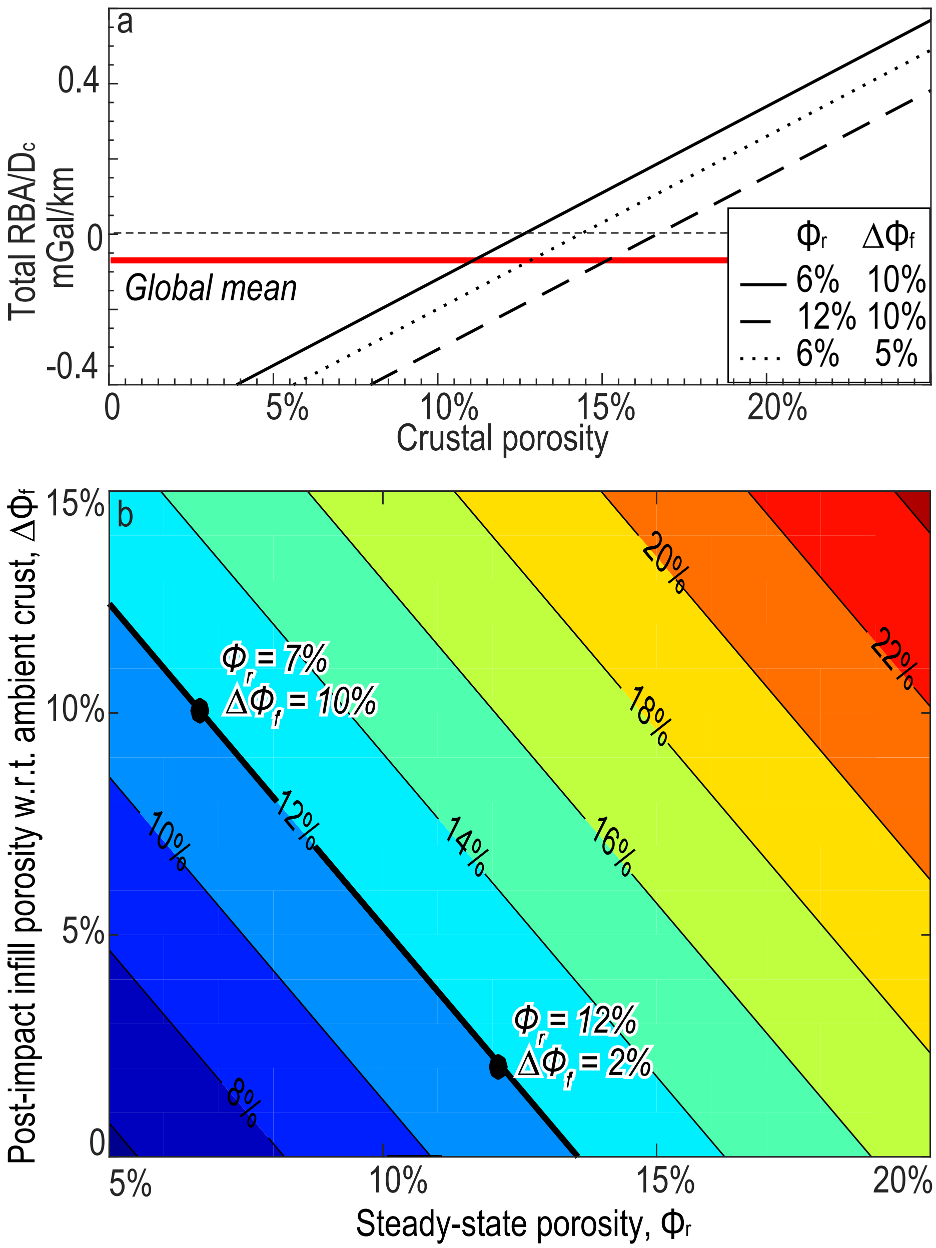

This article is protected by copyright. All rights reserved.